Determination of the exciton singlet-to-triplet ratio in single-layer organic light-emitting diodes

M. Carvelli,[1,2,3,*] R. A. J. Janssen,[1] and R. Coehoorn[1,2]

[1]*Department of Applied Physics, Molecular Materials and Nanosystems, Eindhoven University of Technology, P.O. Box 513, NL-5600 MB Eindhoven, The Netherlands*

[2]*Philips Research Laboratories, High Tech Campus 4, NL-5656 AE Eindhoven, The Netherlands*

[3]*Dutch Polymer Institute, P.O. Box 902, NL-5600 AX Eindhoven, The Netherlands*

(Received 1 February 2010; revised manuscript received 11 November 2010; published 23 February 2011)

The efficiency of fluorescent organic light-emitting diodes (OLEDs) is strongly affected by the fraction of singlet excitons formed. While the standard statistical value of the singlet-to-triplet ratio is 1:3, significant deviations have been reported for several materials, in particular for polymers. We developed a method to determine the singlet fraction with high accuracy for organic semiconductors in single-layer OLEDs by extending a method introduced by Segal *et al.* [Phys. Rev. B **68**, 075211 (2003).] within which the analysis is based on a combination of electroluminescence (EL) and reverse bias photoluminescence (PL) measurements. We carefully determine from a combined experimental and modeling approach the PL and EL emission profiles and light outcoupling efficiencies, which are generally quite different for single-layer devices. The approach is demonstrated for the case of OLEDs based on a blue-emitting polyfluorene-based copolymer, for which the singlet fraction is found to be in the range 10%–25%, increasing with increasing emitting layer thickness but independent of the applied voltage.

DOI: 10.1103/PhysRevB.83.075203 PACS number(s): 71.35.Cc, 78.60.Fi, 72.80.Le

I. INTRODUCTION

In the past decade, various experimental studies have indicated that the singlet exciton formation yield, η_S, in organic light-emitting diodes (OLEDs) can significantly exceed the quantum statistical value of 25%, in particular for polymers.[1–10] It has been suggested[11] that polymer OLEDs based on fluorescent organic semiconductors may therefore become as efficient as phosphorescent OLEDs, within which the otherwise nonradiatively decaying triplet excitons are harvested by making use of heavy-metal-containing co-deposited molecules or copolymerized units. The latter method has made it possible to achieve a near-100% internal quantum efficiency in monochrome small-molecule OLEDs,[12,13] a factor of 4 larger than in fluorescent devices with a singlet-to-triplet ratio of 1:3. However, the issue of the singlet fraction in polymers is still a matter of debate, based on experimental results showing that it is only around 20% for the archetype polyphenylene vinylene (PPV)-based polymer MEH-PPV,[7] on more general considerations of the observed external quantum efficiency of fluorescent polymer OLEDs[7] and on an experimental study which suggests that in a relevant polymer no singlet-triplet interconversion takes place in the exciton precursor (bound polaron pair) states.[14] The occurrence of such interconversion processes is regarded as a crucial condition for obtaining an enhanced singlet fraction.[15–18]

In Table I, an overview is given of the singlet fractions as measured for selected polymers. The methods used may be classified in the following way. The perhaps most direct method (A) involves a determination of the external electroluminescence (EL) quantum efficiency of a complete OLED, η_{EL}, the electron-hole recombination efficiency η_{rec}, the radiative decay efficiency η_{rad}, and the EL light-outcoupling efficiency $\eta_{out,EL}$, using $\eta_S = \eta_{EL}/(\eta_{rec}\eta_{rad}\eta_{out,EL})$. The photoluminescence (PL) quantum yield of single layers on a supporting substrate may be used to estimate η_{rad}. Other methods involve (B) measurements under forward bias of the EL and PL efficiencies of the same device, (C) measurements of the EL efficiency and the voltage dependence of the PL efficiency under reverse bias, (D) EL and PL measurements of the singlet and triplet densities and their dynamics, and (E) optical probing of the effect on the density of photogenerated polarons of resonant microwave radiation, which equalizes the density of singlet and triplet bound polaron pair states. Application of methods D and E requires measurements at cryogenic temperatures, typically 100 K or below, whereas the other methods are applicable at any temperature. These methods have been applied to complete (a) single layer or (b) multilayer OLEDs, on (c) single layers in between noninjecting electrodes or (d) on single layers on a supporting substrate. The materials used were in most cases (I) genuine fluorescent emitters but contained in some studies (II) heavy metal atoms (Pt) in order to enhance the emission from triplet excitons.

Deducing η_S from the absolute EL quantum efficiency (method A) can lead to a relatively high uncertainty. This source of uncertainty is eliminated in methods B–D, which are based on the relative EL and PL intensities measured in the same setup. Within method C, a further refinement is introduced, namely by normalizing the EL intensity by the measured forward current and by normalizing the measured voltage-induced *change* of the PL intensity as measured under reverse bias by the resulting photocurrent. We note that a method for deducing η_S from device studies involving combined EL and PL measurements was already introduced by Kalinowski and co-workers.[19–21] However, in that work on anthracene and tetracene single crystals, no normalization by measured current densities was employed. For the case of OLED structures, the application of methods B–D would (in general) require that a microcavity model is used, as it is possible that the PL and EL light-outcoupling efficiencies are different, resulting from different shapes of the light-absorption and resulting reemission profile (in PL) and the emission profile (in EL). This issue has been recognized by

TABLE I. Overview of measured values of the singlet fraction η_S for selected polymers and of the methods used (see text).

Polymer	η_S (%)	Method	Reference
OC_1C_{10}-PPV	>50	B, a, I	Ref. 1
	>35–45	A, a, I	Ref. 2
	83 ± 7	D, a, I	Ref. 5
Green PPV[a]	>35–45	A, a, I	Ref. 2
MEH-PPV	47	E, d, I	Ref. 3
	20 ± 4	C, b, I	Ref. 7
PtOEP	57 ± 4	D, a, II	Ref. 4
	60	E, d, II	Ref. 9
Polyoctylfluorene (PFO)	57	E, d, I	Ref. 3
	70	D, c, I	Ref. 8
Polyspirobifluorene	44 ± 4	D, a, I	Ref. 10
PF-TAA	10–25	C, a, I	This paper

[a]2-alkoxyphenyl-PPV-co-2,5-dialkoxy-PPV.

several authors. In the work of Segal *et al.* (method C),[7] which for MEH-PPV gives rise to a value of η_S which is quite close to the quantum-statistical value, this uncertainty was strongly reduced by making use of layered OLEDs containing only a relatively thin emissive layer that is well separated from the electrodes, so that the PL and EL outcoupling efficiencies are almost equal. However, when studying more simple single-layer OLEDs, this issue should be taken into account.

In this paper, we investigate in detail the difference between the PL and EL emission profiles in single-layer OLEDs, making use of a recently developed method for accurately determining the EL emission profile from the angular, wavelength, and polarization-resolved emission intensities,[22] and employ this to deduce η_S for single-layer OLEDs using the combined forward bias EL and reverse bias differential PL method introduced by Segal *et al.*[7] Figure 1 shows in a schematic way the method used. In the same setup, a measurement is carried out for the EL intensity P_{EL} (in arbitrary units) per unit of the injected current I_{inj} [Fig. 1(a)] and for the *decrease* of the PL intensity due to field quenching under reverse bias conditions P_{PL} (in the same arbitrary units) per unit of *increase* of the corresponding photocurrent I_{ph} [Fig. 1(b)]. The singlet fraction is expected to be equal to the ratio of these two quantities if the EL and PL light-outcoupling efficiencies, $\eta_{out,EL}$ and $\eta_{out,PL}$, respectively, are equal, and if the recombination efficiency is equal to 1. However, in general the first condition is not met due to the different shapes of the emission profiles. This is shown schematically in Fig. 1. The singlet fraction is therefore given by

$$\eta_S = \frac{1}{\eta_{rec}} \frac{\eta_{out,PL}}{\eta_{out,EL}} \frac{\frac{P_{EL}}{I_{inj}}}{-\frac{dP_{PL}}{dI_{ph}}}. \quad (1)$$

We employed this expression to determine η_S for a polyfluorene-triarylamine copolymer (PF-TAA, described in detail in Sec. II), which is present as a single layer in OLEDs of the type shown in Fig. 1. PF-TAA is a relatively efficient blue fluorescent emitter, with a PL efficiency equal to approximately 60%,[23] and was used in the 13-in. full-color OLED TV display demonstrated by Philips in 2005.[24]

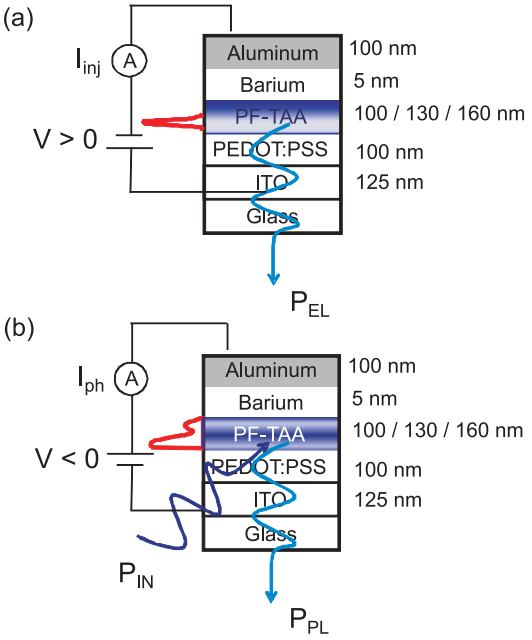

FIG. 1. (Color online) Schematic representation of the method employed to determine the exciton singlet-to-triplet ratio. The same experimental setup is employed to measure (a) the electroluminescence and (b) the photoluminescence at positive and negative voltages, respectively. Combined experimental and modeling approaches are used to calculate the different EL and PL light emission profiles (shown schematically in the figures) and the resulting different light-outcoupling efficiencies. The layer stack is described in more detail in Sec. II.

The hole and electron transport in this material have been intensively studied.[25–27] Its choice is further motivated by the availability of accurate descriptions of the layer thickness and voltage-dependent EL emission profiles.[22] The presence of the copolymerized monomer units, in a small concentration, can give rise to an optimized hole-injection and electron-hole mobility balance, as studied in detail for OLEDs based on various fluorene-based copolymers.[23,28–31] In PF-TAA, the hole states are expected to be localized on these units.[27] The effective conjugation length is therefore expected to be much smaller than in polyfluorene derivatives without copolymerized units, such as polydioctylfluorene (PFO), for which a strongly enhanced singlet efficiency has been found (see Table I). Studies for various types of polymers indicate that η_S should decrease with decreasing repeat length,[4,6,9,32] approaching the quantum-statistical value for systems approaching the monomer limit. For the PF-TAA polymer studied, it is not *a priori* clear whether it could be considered as a material with such a small conjugation length that it would effectively be similar to a small-molecule material, or whether its polymeric character could still give rise to an enhanced singlet fraction. From our results, we deduce values for η_S in the range 10%–25% for PF-TAA, increasing with increasing emitting layer thickness in the 100–160-nm-layer thickness range studied.

Section II contains a more detailed description of the PF-TAA copolymer studied, the experimental setup, and the modeling methods employed. In Sec. III, the experimental

and modeling results are presented and analyzed. Section IV contains a discussion and in Sec. V the conclusions are given.

II. LIGHT-EMITTING POLYMER AND EXPERIMENTAL METHODS

The organic semiconductor studied, PF-TAA, is a blue-emitting polymer from the Lumation™ Blue Series supplied by Sumation Co., Ltd. It consists of a polyfluorene (PF) based polymer with randomly copolymerized triarylamine (TAA) monomer units (7.5 mol %). The molecular structure of the polyfluorene and TAA units is shown in Fig. 2(a). The device structure used is shown in Fig. 1. The anode consists of a 100-nm-thick poly(3,4-ethylenedioxythiophene):poly(styrenesulphonic acid) (PEDOT:PSS) layer, spin-coated on precleaned glass substrates covered with 120 nm indium tin oxide (ITO). The cathode consists of a 5-nm-thick barium and a 100-nm-thick aluminum layer, sequentially evaporated in a high-vacuum chamber on top of the PF-TAA. Devices with three different PF-TAA emitting layer thicknesses, 100, 130, and 160 nm, were studied. The use of patterned bottom and top electrodes results in glass/ITO/PEDOT:PSS/PF-TAA/Ba/Al structures with areas of 1×1 mm^2. The energy-level diagram for the layer stack studied is shown in Fig. 2(b). The electron transport occurs along PF-derived states,[26] while the hole transport takes place via the TAA units.[25,27]

The current (I) versus voltage (V) measurements are carried out using a Keithley 2400 Sourcemeter. The light emitted in the direction orthogonal to the device surface is focused on a cooled Hamamatsu HPD-TA CCD camera. For the PL quenching measurements, a defocused UV diode laser (emission wavelength 405 nm) is used. The optical power on the sample is 0.6 mW. The voltage range within which the forward bias EL measurements were carried out (restricted at the lower side by the instrumental sensitivity and at the higher side by the long-term device stability under steady-state operation) was 8.5–10.5, 9.5–11.5, and 12.5–15.5 V for the 100-, 130-, and 160-nm devices, respectively. All measurements were carried out at room temperature.

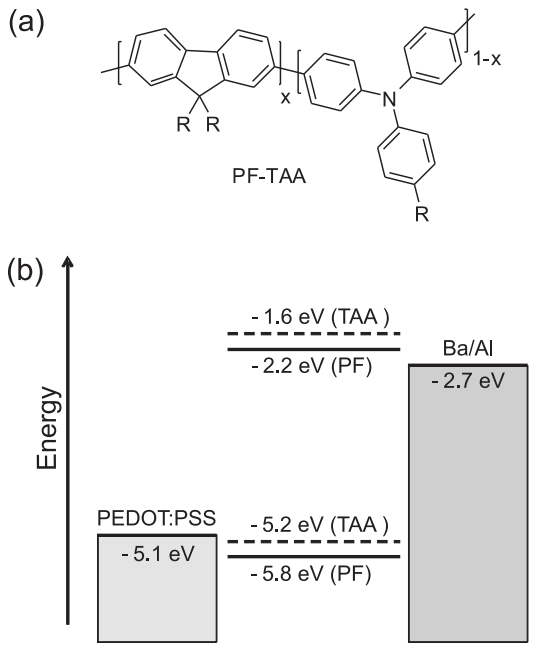

FIG. 2. (a) Molecular structure of PF-TAA, containing randomly copolymerized polyfluorene (PF) and triarylamine (TAA) monomer units (7.5 mol %). (b) Energy-level diagram of the devices studied, with the energies with respect to the vacuum level.

The light absorption in a PL experiment is calculated using a thin-film optical microcavity model (MACLEOD software, Thin Film Center Inc.). The complex refractive indices of the layers are determined by ellipsometry.[22] We first assume that the PL light emission profiles are equal to the absorption profiles. For the devices studied, this is expected to be a fair approximation, as the exciton diffusion length (λ_d) for fluorescent polymers is small, of the order of 5–10 nm.[33] Subsequently, we investigate the possible effect of exciton diffusion on the results of the analysis. The PL outcoupling efficiency is then calculated using a computer simulation tool, LIGHTEX,[34] developed at Philips Research Aachen. The dipole orientation in the PF-TAA layer is assumed to be in plane, as obtained from the analysis of emission experiments in Ref. 22. The microcavity model used treats excitons as radiating dipole emitters and includes absorption in the layers and the enhancement of the radiative decay rate due to nearby electrodes. All optical modes are considered. A comparison with other models described in the literature is given in Ref. 22.

The layer thickness and voltage-dependent EL emission profiles across the active layer were obtained in the manner described in Ref. 22, from the EL emission intensity measured as a function of the wavelength with a resolution of 1 nm, as a function of the emission angle in steps of 2° from orthogonal emission to 70°, and as a function of the polarization, using a commercial Melcher Autronic Display Metrology System (DMS) and using a glass hemisphere on top of the sample to enhance the range of internal modes from which emission can be extracted.[35] LIGHTEX was used to obtain the EL outcoupling efficiencies from these profiles.

III. EXPERIMENTAL RESULTS AND ANALYSIS

In Fig. 3, the experimental results obtained from the EL and PL measurement of a 160-nm-thick device are presented. Similar results were obtained for the 100- and 130-nm devices.

Figure 3(a) shows the dependence of the measured PL quenching $[-\Delta P_{\mathrm{PL}}(V) \equiv P_{\mathrm{PL}}(V) - P_{\mathrm{PL}}(0)]$ and the corresponding photocurrent, $I_{\mathrm{ph}}(V)$, on the reverse applied voltage. The voltage dependence of both quantities is essentially equal, so, as shown in Fig. 3(b), the PL quenching is proportional to the measured photocurrent. The same result was obtained for the 100- and 130-nm devices. The ratio $-dP_{\mathrm{PL}}/dI_{\mathrm{ph}}$ in Eq. (1) is thus independent of the applied voltage, as also observed for other materials in Ref. 7, which confirms the validity of the method.

The consistency of the approach may also be investigated by carrying out a more quantitative analysis of the photocurrent and the photoluminescence change. From the optical power used, the angle of incidence (30° with respect to the surface normal; s-polarized light), and a calculation of the light absorption in the emissive layer, the maximum photocurrent is expected to be 116, 148, and 134 μA for the 100-, 130-, and

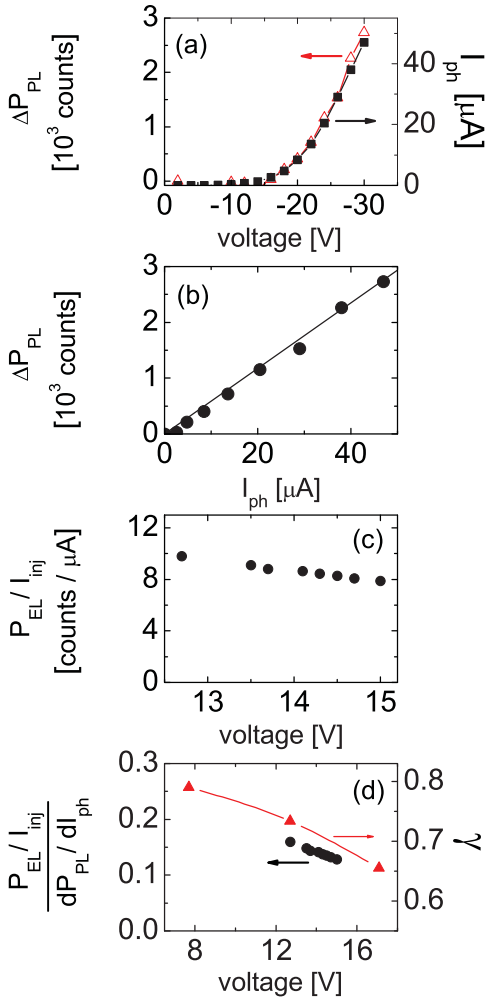

FIG. 3. (Color online) (a) PL quenching and photocurrent as a function of the voltage. (b) Correlation between the measured PL quenching and the corresponding photocurrent for different values of the voltage (solid circles). The line through the origin is a guide to the eye. (c) Voltage dependence of the normalized EL intensity, $P_{\mathrm{EL}}/I_{\mathrm{inj}}$. (d) Voltage dependence of the ratios $(P_{\mathrm{EL}}/I_{\mathrm{inj}})/(-dP_{\mathrm{PL}}/I_{\mathrm{ph}})$ and $\gamma \equiv \eta_{\mathrm{out,EL}}/\eta_{\mathrm{out,PL}}$.

160-nm devices, respectively, with an estimated uncertainty of approximately 20%. From the experimental relative value of the slope of $-\Delta P_{\mathrm{PL}}/P_{\mathrm{PL}}(V=0)$ versus I_{ph}, we deduce values of the maximum photocurrent equal to 93 ± 10, 110 ± 30, and 137 ± 14 μA. Taking the uncertainties of the maximum photocurrents as deduced from both methods into account, we conclude that the experimental results are consistent with the assumption that the PL quenching observed is due to field-induced dissociation of excitons. We note that in all cases the relative PL quenching was at most approximately 40% (by applying a voltage of approximately -18, -24, and -30 V for the 100-, 130-, and 160-nm devices, respectively) to avoid the risk of damaging the devices by the application of a too-high reverse field. We also note that in all cases the slope was obtained from the voltage range in which a significant photoluminescence quenching and a significant photocurrent are measured (e.g., from -20 to -30 V for the 160-nm devices) to be able to determine the slope with a high accuracy.

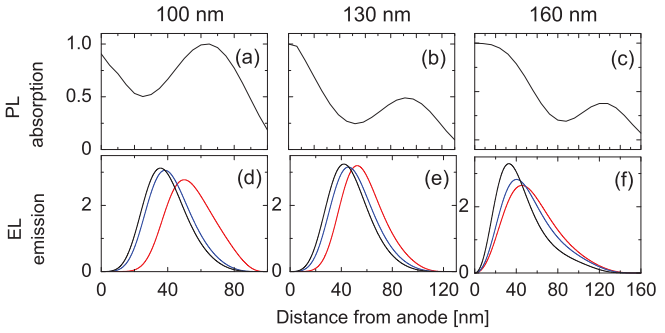

FIG. 4. (Color online) Calculated normalized layer-thickness-dependent (a–c) PL and (d–f) EL emission profiles across the active layer. The voltages used in the EL experiments are 5.3, 8.7, and 11.5 V (100 nm); 6.8, 9.6, and 11.8 V (130 nm); and 7.7, 12.7, and 17.1 V (160 nm). In all devices, the emission profile shifts toward the anode with increasing voltage.

The same experimental setup is employed to measure the optical power and the injected current in an EL experiment. Figure 3(c) shows the measured voltage dependence of the ratio $P_{\mathrm{EL}}/I_{\mathrm{inj}}$ for the 160-nm device, which is proportional to the external quantum efficiency. A weak although not fully negligible rolloff of the external quantum efficiency as a function of the applied voltage is found, which is a well-known phenomenon in fluorescent OLEDs.[36,37] As a result, the ratio $(P_{\mathrm{EL}}/I_{\mathrm{inj}})/(dP_{\mathrm{PL}}/dI_{\mathrm{ph}})$ [see Eq. (1)] depends on the voltage at which the device is driven under EL performance, as shown in Fig. 3(d). This voltage dependence can be understood as a result of a voltage dependence of the EL light-outcoupling efficiency (i.e., of the parameter $\gamma \equiv \eta_{\mathrm{out,EL}}/\eta_{\mathrm{out,PL}}$, which is shown in the same figure). The parameter γ was obtained from the calculated PL emission profiles for each of the three layer thicknesses, shown in Figs. 4(a)–4(c), and from the EL emission profiles as obtained for the three layer thicknesses at the three different voltages for which the profiles are shown in Figs. 4(d)–4(f). The calculated PL emission profiles, which are taken here equal to the absorption profiles, are clearly not homogeneous through the emitting layer due to microcavity effects. Furthermore, they show a distinct emitting layer thickness dependence. The EL emission profiles are not only layer thickness dependent but also slightly voltage dependent. As a result, the parameter γ is found to vary from 1.45 to 1.44 for the 100-nm devices, from 1.30 to 1.15 for the 130-nm devices, and [see Fig. 3(d)] from 0.79 to 0.66 for the 160-nm devices.

The analysis shows that γ can be significantly smaller than 1 (e.g., for the 160-nm-thick emitting layer). This leads to a strong correction to the value of η_{S} that would be obtained if the EL and the PL outcoupling efficiencies were assumed to be equal. Furthermore, the voltage dependence of γ is found for all three thicknesses to be essentially equal to the voltage dependence of the ratio $(P_{\mathrm{EL}}/I_{\mathrm{inj}})/(dP_{\mathrm{PL}}/dI_{\mathrm{ph}})$, as may be seen for the 160-nm devices in Fig. 3(d). It follows from Eq. (1) that the value obtained for η_{S} is then essentially voltage independent, as expected for a material property, if the recombination efficiency is voltage independent. In Sec. IV, we show from numerical studies using a recently developed drift-diffusion device model[38] that for all layer thicknesses

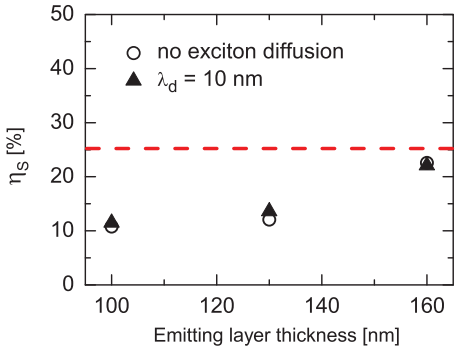

FIG. 5. (Color online) Calculated singlet fraction in PF-TAA as a function of the emitting layer thickness, neglecting exciton diffusion when modeling the PL emission spectrum (circles) and assuming a $\lambda_d = 10$ nm exciton diffusion length (triangles). The standard-statistical singlet fraction is equal to 25%, as indicated by the dashed line.

and voltages $\eta_{\rm rec}$ is indeed very close to 1. This leads to an essentially voltage-independent value for η_S, for all the emitting layer thickness values analyzed. Figure 5 gives the values of the singlet fraction that are deduced for the different emitting layer thicknesses, using the PL and EL emission profiles given in Fig. 4 (circles).

IV. DISCUSSION

The values of the singlet fraction shown in Fig. 5 (circles) are close to the standard statistical value (dashed line) or smaller. To analyze these results, we first consider the effects of exciton diffusion on the PL emission profile. We calculated the PL emission profiles as a function of the exciton diffusion length, assuming as a boundary condition that the electrodes are perfect sinks of excitons, so that the PL emission profile is zero at the electrode interfaces. For realistic values of the diffusion length, up to 10 nm, only a very small and approximately linear variation of the γ parameter is found. In Fig. 5, the values of η_S for a diffusion length of 10 nm are shown (triangles). Although the effect is found to be slightly thickness dependent, and largest for the 130-nm device, it is quite small so it does not explain the observed thickness dependence of η_S.

Second, we investigate to what extent the shape of the EL emission profile shown in Fig. 4 is consistent with the shape which would follow using a drift-diffusion charge transport and recombination simulation. For this purpose, we used the model presented in Ref. 38, using the experimentally determined hole and electron mobility functions obtained in Refs. 25 and 26, respectively. In Ref. 26, the electron mobility was determined using a LiF/Ca/Al cathode, for which the electron injection barrier was found to be $\Phi_e = 0.3 \pm 0.1$ eV. However, in our present study, a Ba/Al cathode is used, for which from a preliminary study Φ_e is estimated to be closer to ~0.5 eV.[23] We investigated the consistency between the experimental results and the model predictions by first comparing the experimental voltage dependence of the current density, J, with the prediction as obtained for $\Phi_e = 0.5$ and 0.6 eV. The results are shown in Fig. 6(a) for 160-nm devices. Below ~3 V, the current density is determined by the leakage current

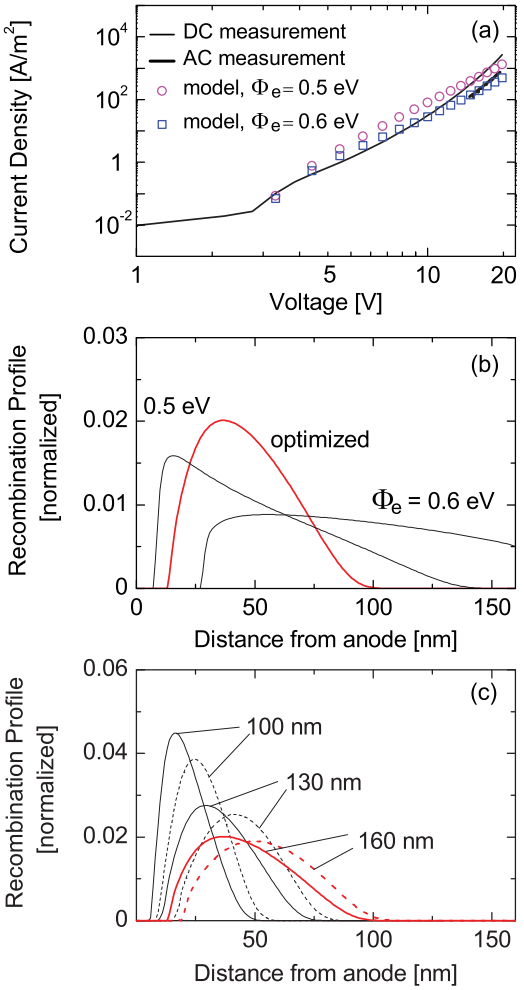

FIG. 6. (Color online) (a) Measured and calculated current density in 160-nm devices, as explained in the main text. (b) Calculated normalized recombination profile for 160-nm devices at 15 V, as obtained using the experimental electron and hole mobility functions and isotropic recombination with $\Phi_e = 0.5$ and 0.6 eV and as obtained using an "optimized" approach (see the main text). (c) Normalized recombination profiles calculated using the optimized approach at 9 and 11 V (100 nm), 10 and 12 V (130 nm), and 13 and 15 V (160 nm). The solid (dashed) curves are for the higher (lower) voltage values.

($J \propto V$). Near the onset voltage, around 3 V, the electron and hole current densities are found to be strongly unbalanced, so the recombination takes place almost exclusively close to the cathode. The current density is therefore almost exclusively due to the hole current density, so it is almost independent of the precise value of the electron injection barrier. This is confirmed by the calculations. The large observed average slope of the $J(V)$ curve at higher voltages, approximately 4, is well predicted by both calculations, although slightly better when assuming $\Phi_e = 0.6$ eV. However, above 10 V, neither of the two curves provides a good description of the slope. From pulsed (ac) measurements (10 Hz at a 1% duty cycle), we found that in this regime some sample heating occurs. Figure 6 reveals a current density increase up to a factor of ~2.5 in the voltage range 13–15 V for which the analysis presented in the previous section was done. It was found

from the simulations that such an effect would correspond to an internal temperature increase of at most ∼25 K and that such a temperature change has (in this case) no significant effect on the shape of the calculated recombination profile. A similar estimated temperature increase was found for the 100- and 130-nm devices, and the same conclusion was obtained concerning the effect on the profiles. The profiles calculated for $\Phi_e = 0.5$ and 0.6 eV, and at 15 V, are shown in Fig. 6(b). A comparison with the experimental profiles shown in Fig. 4(f) shows that the 0.5- and 0.6-eV profiles are located more closely to the anode and cathode, respectively, and that both profiles are significantly wider than as found experimentally. We view this as an indication that a more refined model for the recombination process is required beyond the standard Langevin model employed. Recently, several refinements have been discussed in the literature, including the effect of carrying out the calculation using so-called bipolar mobilities[39] and including the possible effect of mobility anisotropy.[40] An enhanced recombination rate, resulting from an enhanced lateral mobility, would be expected to give rise to narrower recombination profiles. For the PF-TAA polymers that we studied, the presence of a strong in-plane orientation of the emitting dipoles[22] is indicative of a strong in-plane orientation of the polymer chains. A strong anisotropy of the electron mobility, which is due to transport via the lowest unoccupied molecular orbital states derived from the PF backbone, may therefore be expected. However, the hole mobility, which is due to hopping in between the TAA units, is not expected to be strongly anisotropic. To investigate the effect on the recombination profile, we adapted the approach for calculating the local recombination rate presented in Ref. 38 by including an enhanced contribution from lateral hops of electrons to nearest-neighbor sites at which a hole resides. We varied this enhancement factor, considering it as a free parameter, and found that introducing this enhancement indeed gives rise to a narrowing of the profile. For 160-nm devices, we found that the recombination profiles as calculated and measured at 15 V are quite similar when choosing a mobility anisotropy factor equal to 7, using $\Phi_e = 0.5$ eV and using a slightly (factor of 1.5) enhanced electron mobility to fine-tune the peak position. The resulting $J(V)$ curve is almost indistinguishable from that shown in Fig. 6(a) for $\Phi_e = 0.5$ eV. The resulting profile is shown in Fig. 6(b) ("optimized"). The anisotropic shape is quite similar to the experimental profiles measured at 12.7 and 17.1 V. In Fig. 6(c), we investigate the voltage and layer-thickness dependence of the recombination profiles by carrying out calculations for each thickness at two values of the voltage within the experimental voltage range (see Fig. 6 caption). For each case studied, the electron and hole currents are quite well balanced, and the recombination efficiency is found to be essentially equal to 1. Figure 6 shows for all layer thicknesses a predicted shift of the profile toward the anode with increasing voltage. Such a shift is indeed observed, although the experimental shifts are smaller than calculated. Furthermore, the calculations predict for the two thinner devices a peak shift to positions closer to the anode than is actually observed. This might indicate that in these devices close to the anode additional exciton quenching processes take place, on top of the exciton quenching already taken into account in the microcavity model.

A possible explanation of these observations would be a modification of the composition of the PF-TAA near the interface with the PEDOT:PSS layer, giving rise to a reduced radiative lifetime of excitons generated close to the anode. Evidence of proton diffusion at elevated temperatures from the PEDOT:PSS layer into an organic semiconductor deposited on top of that layer was found by Köhnen *et al.*[41] The EL efficiency would be already significantly affected by an approximately 20-nm-thick zone near the anode with a reduced radiative decay probability. We note that in the emission profiles shown in Figs. 4(d)–4(f) such a possible effect would already be included, so in its absence the emission intensities near the anode would be larger. As noted above, the maximum thermal loads in our experiments (∼25 K thermal increase) were quite limited. However, it is not known how the proton diffusion rate into PF-TAA will depend on the temperature.

Another factor that could affect the analysis is polaron or field-induced quenching of singlet excitons,[7] which could result in a decrease of the EL quantum efficiency with increasing current density. However, we have no experimental evidence for this effect. The EL efficiency has been found to show a weak voltage-dependent rolloff, but we have shown that this can be attributed completely to a voltage dependence of the EL outcoupling efficiency. Furthermore, EL-specific losses may occur if electroluminescent excitons form preferentially at certain molecular sites such as charge traps or if excitons preferably recombine at trap sites. As explained by Segal *et al.*,[7] this should result in an EL quantum efficiency that increases with applied voltage when the filling of traps approaches saturation. However, after taking the voltage dependence of the light-outcoupling efficiency into account, we do not find such an increase of the EL quantum efficiency.

Finally, it would be of interest to investigate whether within refined models of the exciton formation and radiative recombination process in OLEDs the recombination efficiency would, for the systems studied, still be very close to 1. One may envisage that (i) the filamentary nature of electron and hole current density[42] due to the energetic disorder and (ii) the screening of the electron-hole attraction by the electrodes might both affect the recombination efficiency when the emission profile is peaked near one of the electrodes. One may also envisage that the generation of excitons at a distance from the electrode which is comparable to the exciton diffusion length could result in a lower effective recombination efficiency. Based on the calculated results shown in Fig. 6(c), this effect would be largest for the thinnest (100-nm) device, because the peak in the calculated recombination profile is located at only approximately 15–25 nm. The trend observed in Fig. 5 would then be consistent with a decrease of the effective recombination efficiency with decreasing device thickness as a result of a decrease of the distance of the peak of the EL recombination profile to the anode. The singlet fraction obtained for the thickest device, which is closer to 25%, would be least affected. Therefore, it could be considered more precise. However, further narrowing down the uncertainty interval of the value of the singlet fraction obtained, by the development of a quantitative model for the recombination profile and exciton quenching near electrodes, is beyond the scope of this paper.

In the absence of a more refined approach from which the observed layer-thickness dependence of the singlet fraction can be explained, our present best estimate is $\eta_S = 17 \pm 6\%$. In view of the significantly enhanced singlet fraction observed for the similar polymer material PFO (see Table I), without hole transporting units, this would indicate that the presence of the TAA monomer units on which the holes are known to be mainly localized makes the effective conjugation length in PF-TAA very short. Strong deviations from the standard statistical value, to higher values, are then less likely.[18,43] We note that a deviation to lower values could be explained within the framework of a model developed by Kalinowski and coworkers,[20,44] who analyzed the effect on the singlet exciton fraction of the trapping of carriers in rather deep states. This would give rise to an activation barrier for singlet exciton generation, thereby reducing the singlet formation rate and thus the EL intensity.

V. CONCLUSIONS

We have extended the method to determine the exciton singlet-to-triplet ratio in OLEDs introduced by Segal *et al.*[7] to single-layer OLEDs, by taking the difference between the light-outcoupling efficiencies in EL and PL experiments into account. The method used to model the outcoupling efficiency in EL and PL experiments is quite general and could also be needed to refine the analyses used in previous studies of the singlet fraction.[1,4,10] For example, the studies of Cao *et al.*[1] and Wilson *et al.*[4] for OC_1C_{10}-PPV and PtOEP, respectively, which are both based on ratios of measured EL and PL intensities, give rise to a seemingly layer-thickness-dependent singlet fraction.

The analysis was applied to a blue-emitting application-relevant polyfluorene-based copolymer, PF-TAA, containing hole-transporting TAA monomer units which give rise to an optimized hole injection and electron-hole mobility balance. Employing the EL emission profile as obtained using a recently developed method from the measured angular-, wavelength-, and polarization-dependent emission intensity,[22] and using the PL emission profile as obtained from optical modeling, it is found that taking the actual EL and PL outcoupling efficiencies into account leads to a singlet fraction in the range 10%–25%, in all cases studied independent of the applied voltage. The maximum attainable internal quantum efficiency of blue fluorescent polymer OLEDs based on PF-TAA is thus severely limited by the unfavorable spin statistics of the exciton formation process.

ACKNOWLEDGMENTS

The authors thank H. Greiner for support when using the LIGHTEX program, P. A. Bobbert and S. L. M. van Mensfoort for useful discussions, and Sumation Co., Ltd., for the supply of Lumation Blue Series polymers. This work forms part of the research program of the Dutch Polymer Institute (Project No. 518). The research has also received funding from the European Community's Seventh Framework program under Grant No. 213708 (AEVIOM, contribution to R.C.).

*marco.carvelli@philips.com

[1] Y. Cao, I. D. Parker, G. Yu, C. Zhang, and A. J. Heeger, Nature (London) **397**, 414 (1999).
[2] J. S. Kim, P. K. H. Ho, N. C. Greenham, and R. H. Friend, J. Appl. Phys. **88**, 1073 (2000).
[3] M. Wohlgenannt, K. Tandon, S. Mazumdar, S. Ramasesha, and Z. V. Vardeny, Nature (London) **409**, 494 (2001).
[4] J. S. Wilson, A. S. Dhoot, A. J. A. B. Seeley, M. S. Khan, A. Köhler, and R. H. Friend, Nature (London) **413**, 828 (2001).
[5] A. S. Dhoot, D. S. Ginger, D. Beljonne, Z. Shuai, and N. C. Greenham, Chem. Phys. Lett. **360**, 195 (2002).
[6] M. Wohlgenannt, X. M. Jiang, Z. V. Vardeny, and R. A. J. Janssen, Phys. Rev. Lett. **88**, 197401 (2002).
[7] M. Segal, M. A. Baldo, R. J. Holmes, S. R Forrest, and Z. G. Soos, Phys. Rev. B **68**, 075211 (2003).
[8] T. Virgili, G. Cerullo, C. Gadermaier, L. Lüer, G. Lanzani, and D. D. C Bradley, Phys. Rev. Lett. **90**, 247402 (2003).
[9] C. Yang, Z. V. Vardeny, A. Köhler, M. Wohlgenannt, M. K. Al-Suti, and M. S. Khan, Phys. Rev. B **70**, 241202(R) (2004).
[10] C. Rothe, S. M. King, and A. P. Monkman, Phys. Rev. Lett. **97**, 076602 (2006).
[11] A. P. Monkman, C. Rothe, and S. M. King, Proc. IEEE **97**, 1597 (2009).
[12] C. Adachi, M. A. Baldo, M. E. Thompson, and S. R. Forrest, J. Appl. Phys. **90**, 5048 (2001).
[13] G. He, M. Peiffer, K. Leo, M. Hofmann, J. Birnstock, R. Pudzich, and J. Salbeck, Appl. Phys. Lett. **85**, 3911 (2004).
[14] M. Reufer, M. J. Walter, P. G. Lagoudakis, A. B. Hummel, J. S. Kolb, H. G. Roskos, U. Scherf, and J. M. Lupton, Nat. Mater. **4**, 340 (2005).
[15] Z. Shuai, D. Beljonne, R. J. Silbey, and J. L. Brédas, Phys. Rev. Lett. **84**, 131 (2000).
[16] M. N. Kobrak and E. R. Bittner, Phys. Rev. B **62**, 11473 (2000).
[17] S. Karabunarliev and E. R. Bittner, Phys. Rev. Lett. **90**, 057402 (2003).
[18] A. Kadashchuk, A. Vakhnin, I. Blonski, D. Beljonne, Z. Shuai, J.-L. Brédas, V. I. Arkhipov, P. Heremans, E. V. Emelianova, and H. Bässler, Phys. Rev. Lett. **93**, 066803 (2004).
[19] J. Kalinowski, J. Godlewski, and J. Glinski, J. Lumin. **17**, 467 (1978).
[20] J. Glinski, J. Godlewski, and J. Kalinowski, Mol. Cryst. Liq. Cryst. **48**, 1 (1978).
[21] J. Kalinowski, Synth. Met. **64**, 123 (1994).
[22] S. L. M. van Mensfoort, M. Carvelli, M. Megens, H. Greiner, D. Wehenkel, M. Bartyzel, R. A. J. Janssen, and R. Coehoorn, Nat. Photonics **4**, 329 (2010).
[23] R. Coehoorn, S. Vulto, S. L. M. van Mensfoort, J. Billen, M. Bartyzel, H. Greiner, and R. Assent, Proc. SPIE **6192**, 61920O (2006).
[24] N. C. Van der Vaart, H. Lifka, F. P. M. Budzelaar, J. E. J. M. Rubingh, J. J. L. Hoppenbrouwers, J. F. Dijksman, R. G. F. A. Verbeek, R. van Woudenberg, F. J. Vossen, M. G. H. Hiddink, J. J. W. M. Rosink, T. N. M. Bernards, A. Giraldo, N. D Young,

D. A. Fish, M. J. Childs, W. A. Steer, D. Lee, and D. S. George, J. Soc. Inf. Disp. **13**, 9 (2005).

[25]S. L. M. van Mensfoort, S. I. E. Vulto, R. A. J. Janssen, and R. Coehoorn, Phys. Rev. B **78**, 085208 (2008).

[26]S. L. M. van Mensfoort, J. Billen, S. I. E. Vulto, R. A. J. Janssen, and R. Coehoorn, Phys. Rev. B **80**, 033202 (2009).

[27]R. J. de Vries, S. L. M. van Mensfoort, V. Shabro, S. I. E. Vulto, R. A. J. Janssen, and R. Coehoorn, Appl. Phys. Lett. **94**, 163307 (2009).

[28]L. C. Palilis, D. G. Lidzey, M. Redecker, D. D. C. Bradley, M. Inbasekaran, E. P. Woo, and W. W. Wu, Synth. Met. **111**, 159 (2000); M. Inbasekaran, E. Woo, W. Wu, M. Bernius, and L. Wujkowski, *ibid.* **111**, 397 (2000).

[29]S. Doi, T. Yamada, Y. Tsubata, and M. Ueda, Proc. SPIE **5519**, 161 (2004).

[30]D. Poplavskyy, W. Su, and F. So, J. Appl. Phys. **98**, 014501 (2005), and references therein.

[31]S. Harkema, R. A. H. J. Kicken, B. M. W. Langeveld-Voss, S. L. M. van Mensfoort, M. M. de Kok, and R. Coehoorn, Org. Electron. **11**, 755 (2010).

[32]J. Cabanillas-Gonzalez, M. R. Antognazza, T. Virgili, G. Lanzani, C. Gadermaier, M. Sonntag, and P. Strohriegl, Phys. Rev. B **71**, 155207 (2005).

[33]D. E. Markov and P. W. M. Blom, Phys. Rev. B **72**, 161401(R) (2005).

[34]H. Greiner and O. J. F. Martin, Proc. SPIE **5214**, 248 (2004).

[35]It was found after the publication of Ref. 22 that an angular-dependent correction should be applied to the measured EL intensities. The corrected profiles are shown in Fig. 4. For the 100- and 130-nm devices, the emission peak is found to be at a slightly larger distance from the anode for all three voltages considered, whereas for the 160-nm device the change of the profile is very small.

[36]N. C. Giebink and S. R. Forrest, Phys. Rev. B **77**, 235215 (2008).

[37]E. A. Meulenkamp, R. van Aar, J. J. A. M. Bastiaansenc, A. J. M. van den Biggelaar, H. Börner, K. Brunner, M. Büchel, A. van Dijken, N. M. M. Kiggen, M. Kilitziraki, M. M. de Kok, B. M. W. Langeveld, M. P. H. Ligter, S. I. E. Vulto, P. van de Weijer, and S. H. P. M. de Winter, Proc. SPIE **5464**, 90 (2004).

[38]R. Coehoorn and S. L. M. van Mensfoort, Phys. Rev. B **80**, 085302 (2009).

[39]J. J. M. van der Holst, F. W. A. van Oost, R. Coehoorn, and P. A. Bobbert, Phys. Rev. B **80**, 235202 (2009).

[40]C. Groves and N. C. Greenham, Phys. Rev. B **78**, 155205 (2008).

[41]A. Köhnen, N. Riegel, J. H.-W. Kremer, H. Lademann, D. C. Müller, and K. Meerholtz, Adv. Mater. **21**, 879 (2009).

[42]J. J. M. van der Holst, M. A. Uijttewaal, B. Ramachandhran, R. Coehoorn, P. A. Bobbert, G. A. de Wijs, and R. A. de Groot, Phys. Rev. B **79**, 085203 (2009).

[43]D. Beljonne, A. Ye, Z. Shuai, and J.-L. Brédas, Adv. Funct. Mater. **14**, 684 (2004).

[44]J. Kalinowski, *Organic Light Emitting Diodes: Principles, Characteristics and Processes* (Dekker, New York, 2005).